

REDSHIFTED 21CM SIGNATURES AROUND THE HIGHEST REDSHIFT QUASARS

J. STUART B. WYITHE¹ AND ABRAHAM LOEB²
 swyithe@isis.ph.unimelb.edu.au; aloeb@cfa.harvard.edu
 Draft version October 31, 2018

ABSTRACT

The Ly α absorption spectrum of the highest redshift quasars indicates that they are surrounded by giant H II regions, a few Mpc in size. The neutral gas around these H II regions should emit 21cm radiation in excess of the Cosmic Microwave Background, and enable future radio telescopes to measure the transverse extent of these H II regions. At early times, the H II regions expand with a relativistic speed. Consequently, their measured sizes along the line-of-sight (via Ly α absorption) and transverse to it (via 21 cm emission) should have different observed values due to relativistic time-delay. We show that the combined measurement of these sizes would directly constrain the neutral fraction of the surrounding intergalactic medium (IGM) as well as the quasar lifetime. Based on current number counts of luminous quasars at $z \gtrsim 6$, an instrument like *LOFAR* should detect $\gtrsim 2$ redshifted 21cm shells per field (with a radius of 11°) around active quasars as bright as those already discovered by SDSS, and $\gtrsim 200$ relic shells of inactive quasars per field. We show that Ly α photons from the quasar are unable to heat the IGM or to couple the spin and kinetic temperatures of atomic hydrogen beyond the edge of the H II region. The detection of the IGM in 21cm emission around high redshift quasars would therefore gauge the presence of a cosmic Ly α background during the reionization epoch.

Subject headings: cosmology: theory - intergalactic medium - quasars: general - radio lines: general

1. INTRODUCTION

The recent discovery of quasars at $z > 6$ (Fan et al. 2001; Fan et al. 2003) and the subsequent observation of two Gunn-Peterson (1965) troughs (Djorgovski et al. 2003; White et al. 2003) established a new era in studies of the end of the reionization epoch. The absorption of Ly α photons from these quasars probes the ionization state of the hydrogen in the intergalactic medium (IGM) near the quasar redshift and has revealed giant ionized regions (Cen & Haiman 2000; Madau & Rees 2000). Comparison of the radii of these regions with the ionizing flux implies quasar ages of $\lesssim 10^7$ years, and an ionization front that is expanding with a relativistic speed (Wyithe & Loeb 2004).

The generation of planned low frequency instruments (such as *LOFAR*³ or the *SKA*⁴) will open a new window on the state of hydrogen in the pre-reionization universe through the emission or absorption of 21cm photons relative to the Cosmic Microwave Background (CMB) by neutral hydrogen in the IGM (Scott & Rees 1990; Madau, Meiksin & Rees 1997; Gnedin & Ostriker 1997; Shaver et al. 1999; Tozzi et al. 2000; Iliev et al. 2002, 2003; Ciardi & Madau 2003; Furlanetto, Sokasian & Hernquist 2003; Zaldarriaga, Furlanetto, & Hernquist 2003; Gnedin & Shaver 2003; Loeb & Zaldarriaga 2003). The giant H II regions surrounding the highest redshift quasars should be visible via rings of redshifted 21cm emission from warm but neutral gas beyond the ionization front.

The relativistic expansion of the H II region implies that the radii measured along and transverse to the line-of-sight using the Ly α and 21cm techniques respectively, probe different epochs due to relativistic time delay. In this paper

we discuss what will be learned about the state of the IGM surrounding the highest redshift quasars by combining Ly α and 21cm measurements. In § 2 we discuss the measurements of radii of the H II region in Ly α absorption and redshifted 21cm emission. The relation between these radii and the neutral fraction of the IGM are then discussed in § 3. Some examples of the brightness temperature profiles around high redshift quasars are presented in § 4. In § 5 we discuss the observation of fossil H II regions and their utility as a probe of the radiation background at high redshift. Finally in § 6 we discuss the utility of quasar Strömgen spheres in the calibration of the global signature of reionization. § 7 summarizes our main results. Throughout the paper we adopt the set of cosmological parameters determined by the *Wilkinson Microwave Anisotropy Probe* (WMAP, Spergel et al. 2003), namely mass density parameters of $\Omega_m = 0.27$ in matter, $\Omega_b = 0.044$ in baryons, $\Omega_\Lambda = 0.73$ in a cosmological constant, and a Hubble constant of $H_0 = 71 \text{ km s}^{-1} \text{ Mpc}^{-1}$.

2. OBSERVATIONS OF STRÖMGREN SPHERES IN REDSHIFTED 21CM EMISSION AND LY α ABSORPTION

First, we consider the observed signatures of H II regions (Strömgen spheres) around the highest redshift quasars during their early relativistic expansion.

2.1. *Evolution of the Strömgen Sphere Around a High Redshift Quasar*

Neglecting recombinations which do not become important until the expansion becomes sub-relativistic, White et al. (2003) derived the evolution of the physical radius of the Strömgen Sphere (R_p) as a function of the source age

¹ University of Melbourne, Parkville, Victoria, Australia

² Harvard-Smithsonian Center for Astrophysics, 60 Garden St., Cambridge, MA 02138

³ See <http://www.lofar.org>

⁴ See <http://www.skatelescope.org>

(t_{age}) which can be easily extended to include the possibility of a non-zero radius (R_0) at the initial time $t_{\text{age}} = 0$,

$$\dot{N} \left(t_{\text{age}} - \frac{R_p}{c} \right) = \frac{4\pi}{3} (R_p^3 - R_0^3) x_{\text{HI}} n_{\text{H}}^0 (1+z)^3, \quad (1)$$

where \dot{N} is the production rate of ionizing photons by the quasar, n_{H}^0 is the co-moving hydrogen number density, x_{HI} is the neutral fraction and c is the speed of light. This cubic equation may be solved algebraically (White et al. 2003). Alternatively, R_p may be found by integrating the differential equation

$$\frac{dR_p}{dt} = c \left(\frac{\dot{N}}{\dot{N} + 4\pi R_p^2 c x_{\text{HI}} n_{\text{H}}^0 (1+z)^3} \right), \quad (2)$$

with the initial condition $R_p(0) = R_0$. The latter approach (Wyithe & Loeb 2004) allows for the inclusion of recombinations. As long as the number of photons emitted per time interval Δt is larger than the number of hydrogens in a shell of thickness $\Delta R = c\Delta t$ at R_p , the H I region continues to expand at nearly the speed of light.

Calculations of R_p in this paper assume that the ionization front is thin. The spectrum averaged mean-free path for the ionizing quasar photons is $\lambda \sim 1.5 x_{\text{HI}}^{-1} (1+z)^{-3} \text{Mpc}$, which may be compared to the bubble radius $R_p \sim 4.5 \text{Mpc}$, to yield the fractional thickness of the ionization front $f \equiv (\lambda/R_p) \sim 2 \times 10^{-3} (R_p/4.5 \text{Mpc})^{-1} x_{\text{HI}}^{-1} [(1+z)/7.3]^{-3}$. The assumption of a thin ionization front may be considered reasonable provided that $x_{\text{HI}} \gtrsim 10^{-2}$. A low neutral fraction is unlikely given the size of the observed H II regions ($R_p \sim 4.5 \text{Mpc}$) around the $z \gtrsim 6.3$ quasars (Wyithe & Loeb 2004). X-ray photons have a longer mean free path but are rare and do not contribute significantly to the number of ionizations.

2.2. The Strömgren Sphere Radius Measured Through Ly α Absorption

Equations (1) and (2) refer to the Strömgren sphere radius at a time t_{age} after the source turns on. However measurements of the radius through Ly α absorption (R_{Ly}) are made along the line of sight. Ly α photons emitted at t_{age} are not absorbed until a time t satisfying the relation $t = t_{\text{age}} + R(t)/c$ (note that the quasar may no longer be active at t). When considering the value of R_{Ly} measured through Ly α absorption, the relevant time to consider is therefore the age of the quasar at the time when the photons being absorbed at the edge of the H II region were emitted $t_{\text{age,e}} = t_{\text{age}} - R(t_{\text{age}})/c$. In the absence of recombinations (White et al. 2003), the relation between R_{Ly} and $t_{\text{age,e}}$ is equivalent to the infinite speed of light solution for the evolution of a Strömgren sphere radius (Haiman & Cen 2000; Madau & Rees 2000),

$$R_{\text{Ly}} = \left(R_0^3 + \frac{3}{4\pi} \frac{\dot{N}_{\parallel} t_{\text{age,e}}}{x_{\text{HI}} n_{\text{H}}^0 (1+z)^3} \right)^{1/3} = 4 \text{Mpc} \left[\left(\frac{R_0}{3.2 \text{Mpc}} \right)^3 + \left(\frac{\dot{N}_{\parallel}}{10^{57} \text{s}^{-1}} \right) \left(\frac{t_{\text{age,e}}}{10^7 \text{yr}} \right) \left(\frac{1+z}{7.5} \right)^{-3} \right]^{1/3}$$

where we add the subscript \parallel to denote the isotropic equivalent value of \dot{N} for a measurement done parallel to the line-of-sight.

2.3. The Strömgren radius measured through H I emission and absorption

Madau, Meiksin & Rees (1997), and Tozzi et al. (2000) have considered the H I signature of the IGM surrounding a high redshift quasar. Outside the H II region, neutral hydrogen may be heated by soft X-rays and by scattering of Ly α photons. The spin temperature of the neutral hydrogen is coupled to the kinetic temperature of the IGM through Ly α scattering of a background of UV photons, and results in 21cm emission (in excess of the CMB flux) around the quasar.

2.3.1. The Ly α Scattering rate

The spin temperature of a warm IGM quickly becomes coupled to the CMB radiation, so that it yields no contrast for H I observations (Madau, Meiksin & Rees 1997). However scatterings of Ly α photons couple the spin temperature of the warm IGM at radii $R > R_p$ through the Wouthuysen-Field effect (Wouthuysen 1952; Field 1958). The spin temperature

$$T_S = \frac{T_{\text{CMB}} + y_{\alpha} T_{\text{IGM}}}{1 + y_{\alpha}} \quad (3)$$

is weighted between the CMB temperature and the IGM temperature through the Ly α pumping efficiency

$$y_{\alpha} \equiv \frac{4P_{\alpha} T_{\star}}{27A_{10} T_{\text{IGM}}}. \quad (4)$$

In equation (4), $T_{\star} = 0.068 \text{K}$ is the temperature corresponding to the transition energy, $A_{10} = 2.85 \times 10^{-15} \text{s}^{-1}$ is the spontaneous decay rate of the hyperfine transition, and P_{α} is the Ly α scattering rate per hydrogen.

The value of P_{α} may be calculated for a continuum UV source embedded in an expanding IGM around a Strömgren sphere as follows (see Loeb & Rybicki 1999 for more details on the related physics). In the absence of scattering, photons that start at a frequency separation $\Delta\nu$ on the blue side of the Ly α resonance frequency ν_{α} would redshift into resonance at some distance $R_{\text{res}} = (\Delta\nu/\nu_{\alpha})c/H$ from the source, where $H = H(z)$ is the Hubble parameter at the quasar redshift. At this distance, the Hubble velocity of the IGM introduces a Doppler shift that is equal to the initial blueshift of these photons relative to the Ly α line center. When a resonant photon enters the neutral IGM near R_{res} , its mean-free-path becomes very short because of the large cross-section to Ly α scattering. As the photon frequency redshifts very close to the Ly α resonance, the mean-free-path diminishes, and the frequency shift per scattering (which corresponds to the Hubble velocity increment across a mean-free-path) goes to zero. Consequently, the photon spends a very long time around R_{res} . At this stage, the finite temperature of the gas becomes important. The photons are able to diffuse out of resonance primarily due to the Doppler shifts they encounter by the thermal speed of the atoms at R_{res} .

Each scattering near R_{res} leads to a fractional frequency shift by the thermal Doppler effect of $\Delta\nu_{\text{th}}/\nu_{\alpha} = v_{\text{th}}/c$, where $v_{\text{th}} = (2kT_{\text{IGM}}/m_p)^{1/2}$ is the thermal speed of the atoms and ν_{α} is the resonant Ly α frequency. The thermal shifts are of random sign and so the photons go through a random walk in frequency. Consider the photons just

around the resonant frequency at R_{res} . These photons change their frequency by $\sim \Delta\nu_{\text{th}}$ in each scattering, and have a mean free path of $\lambda_{\text{th}} = 1/[n_{\text{H}}^0(1+z)^3\sigma_{\text{th}}]$. Here σ_{th} is the Ly α cross-section at the center of the thermally broadened Ly α line (Rybicki & Lightman 1979)

$$\sigma_{\text{th}} = \frac{\sqrt{\pi}e^2}{m_e c} \frac{f_{12}}{\Delta\nu_{\text{th}}} = 5.87 \times 10^{-12} \text{cm}^2 \left(\frac{T_{\text{IGM}}}{1 \text{K}} \right)^{-1/2}, \quad (5)$$

where e and m_e are the electron charge and mass, and f_{21} is the oscillator strength for the Ly α transition. The mean intensity of nearly resonant photons at R_{res} is increased by a factor of $\sim l/\lambda_{\text{th}}$ relative to optically-thin conditions, where l is the so-called Sobolev length, defined as the distance over which the bulk velocity gradient of the medium equals the thermal speed of an atom,

$$l = \frac{v_{\text{th}}}{dv/dR} = \frac{v_{\text{th}}}{H}, \quad (6)$$

and $v = HR$ is the Hubble velocity. The optical-depth factor $\tau_{\text{th}} = l/\lambda_{\text{th}}$ reflects the fact that the diffusion speed of photons across the resonance region of width $\sim l$ is a factor λ_{th}/l times smaller than the speed of light.

In a steady state, the mean intensity at all radii should therefore be enhanced relative to the optically-thin case by a factor of $\sim \tau_{\text{th}}$. However, a steady state will not be established immediately when light from the quasar first penetrates the neutral IGM because of the slow diffusion speed of the resonant photons. At early times, scattering will produce an exponential reduction in resonant photon flux by a factor $\propto e^{-\tau_{\text{th}}}$. Even though photons may be sufficiently blue that they do not redshift into the resonance until R_{res} , they would still be absorbed by the blue wing of the Ly α resonance (where the cross-section is still considerable) at radii smaller than R_{res} .

Let us therefore consider photons of arbitrary frequency on the blue side of the Ly α resonance and calculate their mean intensity at R_{res} . We define the mean intensity as the angular average of the specific (directional) intensity $I(\nu, \mu)$, namely $J(\nu) = \frac{1}{2} \int_{-1}^1 d\mu I(\nu, \mu)$ where $\mu = \cos\theta$ is the direction relative to the radius vector at R_{res} (Loeb & Rybicki 1999). The Ly α optical depth for photons with frequency ν at a radius R_{res} is

$$\tau(\nu) = \int_{R_{\text{res}} - \Delta R_{\text{pl}}}^{R_{\text{res}}} dR' \sigma_{\alpha} \left(\nu \left[1 + \frac{H}{c} (R_{\text{res}} - R') \right] \right) n_{\text{H}}^0 (1+z)^3, \quad (7)$$

where $\sigma_{\alpha}(\nu) = \sigma_{\text{th}} \exp\{-\nu(\nu - \nu_{\alpha})^2 / \Delta\nu_{\text{th}}^2\}$ is the thermally-broadened cross-section (Rybicki & Lightman 1979), and $\Delta R_{\text{pl}} = R_{\text{res}} - R_{\text{p}}(t - \Delta t)$ is the path-length traversed by a photon through the neutral IGM after it had crossed the boundary of the H II region at a time $t - \Delta t$. In the strong scattering regime ($\tau(\nu) \gg 1$), the mean intensity is a factor of $\tau(\nu)$ larger than the specific intensity along the radial direction, because the radial diffusion speed of the photons is $\sim c/\tau(\nu)$. The initial mean intensity of nearly resonant photons at radius R_{res} is therefore

$$J(\nu) \sim \frac{1}{4\pi R_{\text{res}}^2} \epsilon_{\text{local}}(\nu) \tau(\nu) e^{-\tau(\nu)}, \quad (8)$$

where

$$\epsilon_{\text{local}}(\nu) = \epsilon \left(\nu \left(1 + \frac{HR_{\text{res}}}{c} \right) \right) \left[\frac{HR_{\text{res}}}{c} + 1 \right]^{-1} \quad (9)$$

⁵ Note that the diffusion speed of a photon is a function of time as its frequency drifts in and out of resonance with the Ly α transition of the expanding IGM.

is the redshifted source spectrum $\epsilon(\nu)$ in $\text{erg s}^{-1} \text{Hz}^{-1}$. The scattering rate P_{α} may then be calculated from the mean intensity as

$$P_{\alpha} = \int_0^{\infty} d\nu \frac{J(\nu)}{h_{\text{p}}\nu} \sigma_{\alpha}(\nu). \quad (10)$$

The directional intensity of resonant Ly α photons starts high near the boundary of the H II region at R_{p} , but is initially suppressed at larger radii. Resonant photons will diffuse to radii larger than R_{p} at a speed $\sim c/\tau_{\text{th}}$. In the case of a stationary H II front, the high intensity region expands with time, extending a distance $(c/\tau_{\text{th}})\Delta t$ beyond the edge of the H II region after a time Δt , and absorption will truncate the intensity at radii larger than $R_{\text{p}} + (c/\tau_{\text{th}})\Delta t$. For the quasars under consideration the expansion speed of the H II region ($\gtrsim 0.1c$) is well in excess of the diffusion speed⁵ of resonant Ly α photons ($c/\tau_{\text{th}} \sim 10^{-5}c$). On the timescales of interest here, there is a deficit of photons near the line center as described by equation (8).

The critical thermalization rate above which Ly α scattering couples T_{S} to T_{IGM} is given by (Madau, Meiksin & Rees 1997)

$$P_{\text{th}} \equiv \frac{27A_{10}T_{\text{CMB}}}{4T_{\star}} \sim 5 \times 10^{-12} \left(\frac{1+z}{7.5} \right) \text{s}^{-1} \quad (11)$$

We find that P_{α} only exceeds the thermalization rate P_{th} within a negligibly thin shell around the H II region ($\lesssim 10^{-4} \text{Mpc}$). As a result, detection of redshifted 21cm emission from the H II regions of quasars will require the presence of a UV background. Background photons between the Ly α and the Lyman-limit frequencies can propagate through the universe and redshift with time to the point where they resonate with the Ly α line and couple T_{S} to T_{K} . Such a background is expected to be present at $z \sim 6.5$ since the large electron scattering optical depth measured by WMAP (Kogut et al. 2003) implies that the IGM had been significantly reionized by that time (requiring the production of more than one ionizing photon per baryon above the Lyman-limit).

Our result for the scattering rate should be compared with the result of Madau, Meiksin & Rees (1997) who estimated

$$P_{\alpha} = \int_0^{\infty} d\nu \frac{\epsilon(\nu)}{h_{\text{p}}\nu} \frac{1}{4\pi R^2} \sigma_{\alpha}(\nu) \quad (12)$$

$$\sim (8 \times 10^{-11} \text{s}^{-1}) \left(\frac{R}{1 \text{Mpc}} \right)^{-2} \left(\frac{\nu_{\alpha} \epsilon(\nu_{\alpha})}{3 \times 10^{46} \text{erg s}^{-1} \text{Hz}^{-1}} \right).$$

In the steady state this expression incorrectly neglects the rise in intensity that follows from the small diffusion speed of photons near the Ly α resonance and hence underestimates the value of P_{α} by a factor of $\sim n_{\text{H}}^0(1+z)^3\sigma_{\text{th}}v_{\text{th}}/H$ which amounts to several orders of magnitude. However, in the initial state the expression neglects the absorption of resonant photons before they reach a radius $R > R_{\text{p}}$, and so overestimates the value of P_{α} outside the H II region by several orders of magnitude.

The scattering of Ly α photons may also provide a source of heating for the gas. As this peak shifts to longer wavelengths, it loses energy to the hydrogen atoms off which

the photons scatter (Chen & Miralda-Escude 2003). The additional energy density due to the scattering is

$$U = \frac{\epsilon_{\text{local}}(\nu_{\alpha})}{4\pi R^2 c} \left(\frac{l}{\lambda} - 1 \right) \Delta\nu_{\text{th}} \sim P_{\alpha} \frac{h_{\text{p}}\nu_{\alpha}}{c\sigma_{\text{th}}}. \quad (13)$$

The rate at which energy is lost from the line in an expanding IGM equals the heating rate of the gas. Hence we have

$$\Gamma_{\alpha} = \frac{dU}{dt} = U \frac{1}{\nu} \frac{d\nu}{dt} = HP_{\alpha} \frac{h_{\text{p}}\nu_{\alpha}}{c\sigma_{\text{th}}}. \quad (14)$$

This heating rate, which is proportional to the Ly α scattering rate, does not contribute to the heating of gas outside the H II region owing to the very low Ly α intensity there. Instead, the heating is dominated by X-rays which we discuss next.

2.3.2. X-ray Heating Beyond the H II Region

Gas in the IGM outside the ionized region is subject to secondary electron heating resulting from ionizations by soft X-rays that propagate into the neutral IGM beyond the H II region. The heating rate Γ_{x} in $\text{erg s}^{-1} \text{Mpc}^{-3}$ at radius $R > R_{\text{p}}$ due to a source with a spectrum $\epsilon(\nu)$ (in erg/sec/Hz) is

$$\Gamma_{\text{x}}(R, t) = \int_{\nu_{\text{ion}}}^{\infty} d\nu f_{\text{x}} \frac{\epsilon_{\text{local}}(\nu)}{4\pi R^2} \sigma_{\text{pi}}(\nu) x_{\text{HI}} n_{\text{H}}^0 (1+z)^3 \times \exp[-\Delta R_{\text{pl}} \sigma_{\text{pi}}(\nu) x_{\text{HI}} n_{\text{H}}^0 (1+z)^3], \quad (15)$$

where $\sigma_{\text{pi}}(\nu)$ is the cross-section for photoionization and $\nu_{\text{ion}} = 3.29 \times 10^{15} \text{Hz}$ is the Lyman-limit frequency corresponding to the ionization threshold of hydrogen. In equation (15) $\Delta R_{\text{pl}} = R - R_{\text{p}}(t - \Delta t)$ is the path-length of a photon through the neutral IGM after it crossed the boundary of the H II region at time $t - \Delta t$. We have neglected adiabatic cooling due to cosmological expansion in this expression since the quasar lifetime is much shorter than the Hubble time. The fraction of photon energy converted into heat, f_{x} , may be evaluated using the fitting formula (Shull & van Steenberg 1985)

$$f_{\text{x}} = 0.9971 \left(1 - [1 - (1 - x_{\text{HI}})^{0.2663}]^{1.3163} \right). \quad (16)$$

This equation is valid for photon energies $h_{\text{p}}\nu \gtrsim 100\text{eV}$. At lower energies, the value of f_{x} may be roughly approximated by multiplying equation (16) with an additional factor of $\exp([100\text{eV} - h_{\text{p}}\nu]/100\text{eV})$ (with the constraint that $f_{\text{x}} < 1$). The residual ionization fraction from cosmological recombination of $\sim 5 \times 10^{-4}$ yields $f_{\text{x}} \sim 0.17$ (Madau et al. 1997), which sets the minimum heating rate. The heating rate leads to a temperature rise according to

$$\frac{dT_{\text{IGM}}}{dt} = \frac{2}{3} \frac{\Gamma_{\text{x}}}{k_{\text{B}}} \frac{1}{x_{\text{HI}} n_{\text{H}}^0 (1+z)^3}. \quad (17)$$

2.3.3. Redshifted 21cm Observation of Quasar H II Regions

The above discussion has shown that X-rays from the quasar are capable of heating the gas outside the H II region, and that the spin temperature of this warm gas can be coupled to its kinetic temperature in the presence of a strong UV (Ly α) background. In regions of the IGM where the spin temperature is decoupled from the CMB temperature, a differential antenna temperature of

$$\delta T_{\text{b}} = (23\text{mK}) x_{\text{HI}} \left(\frac{1+z}{7.5} \right)^{1/2} \left(\frac{T_{\text{S}} - T_{\text{CMB}}}{T_{\text{S}}} \right) \quad (18)$$

is observed. In equation (18) we have assumed a uniform IGM at the mean density with a neutral fraction x_{HI} . The luminous high redshift quasars reside in rare high-density regions. However on the scale of several Mpc, the overdensity due to infall around these regions is $\lesssim 10\%$ (Barkana & Loeb 2003a).

The brightness temperature of the redshifted 21cm signal is small and subject to severe foreground contamination problems. Studies by Di Matteo et al. (2002), and Oh & Mack (2003) have found that on scales of several arcminutes, randomly distributed point sources would have to be removed down to a level of $\sim 1\mu\text{Jy}$ before brightness temperature fluctuations of order 10 mK could be detected. In the presence of the expected level of clustering of these sources, even the removal of point sources below $1\mu\text{Jy}$ would leave foreground fluctuations on this scale that are several orders of magnitude in excess of the redshifted 21cm signal. However, the spectrum of the foreground contaminants is expected to be smooth (Shaver et al. 1999). The width of the H II region corresponds to a recessional velocity $v \lesssim 3000 \text{km s}^{-1}$ or a redshift interval of $\sim (1+z)v/c \sim 0.07$. The redshifted 21cm ring will therefore produce a bump (or a dip) on top of the smooth foreground spectrum at the redshift of the quasar.

At a frequency $\nu_{\text{bp}} \sim 120\text{MHz}$, an instrument like *LO-FAR* is expected to have a band-pass of $\Delta\nu_{\text{bp}} \sim 4\text{MHz}$. This should be compared with the frequency shift associated with the redshift difference between light emitted at the quasar and the edge of the H II region along the line of sight

$$\Delta\nu \sim 2\text{MHz} \left(\frac{R_{\text{Ly}}}{4\text{Mpc}} \right) \left(\frac{1+z}{7.5} \right). \quad (19)$$

Since many channels are contained within each band-pass, the structure of the H II region can therefore be probed along the line-of-sight in frequency space (Madau, Meiksin & Rees 1997), allowing determination of the full three dimensional shape of the H II region, including the radius of the H II region behind the quasar in addition to the radius R_{Ly} of the H II region in front of the quasar.

There are two distinct possibilities for the redshifted 21cm signature of a high redshift H II region. First, the region might be expanding into a cold IGM, in which case emission will only be seen out to a radius where the warming X-rays can reach. Alternatively, the IGM may have been pre-heated, either by an X-ray background, by gravitationally induced shocks in the IGM (Furlanetto & Loeb 2003), or by an early reionization (e.g. Wyithe & Loeb 2003a; Cen 2003). The presence of Gunn-Peterson troughs in quasar spectra at $z \gtrsim 6$ implies an IGM that is at least partially neutral, while the relatively small sizes of the Strömgen spheres around these quasars suggest a neutral fraction that is of order unity (Wyithe & Loeb 2004). On the other hand, observations from WMAP (Kogut et al. 2003) suggest an optical depth to electron scattering of $\tau \sim 0.17$ and therefore significant reionization at $z \sim 20$. If the universe were reionized twice, then the Strömgen spheres would be expanding into a partially neutral, but warm IGM.

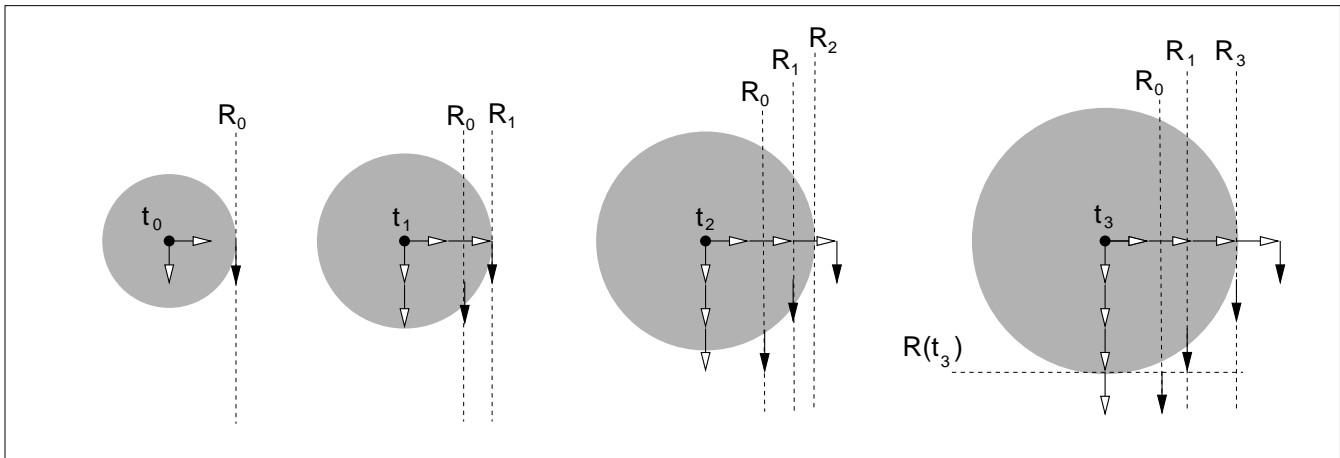


FIG. 1.— Schematic illustration of the geometry of Ly α and redshifted 21cm observations of a relativistically expanding quasar Strömgren sphere (dark regions). The four panels show the evolution at 4 different times. The quasar turns on at t_0 , emitting photons isotropically into a pre-existing H II region of radius R_0 . Ly α photons (open arrows) emitted at t_0 reach the edge of the H II region at t_1 . At that time, 21cm photons (closed arrows) are emitted by the heated gas perpendicular to the line-of-sight (at the quasar redshift) at $R > R_0$ and travel towards the observer. At t_3 , the Ly α photons emitted at t_1 reach the edge of the H II region. The absorption of these photons encodes a measurement of R_3 . When these photons are observed, they are accompanied by 21 cm photons (emitted at t_1 from the quasars redshift), which show a ring of radius R_0 .

3. COMPARISON OF STRÖMGREN SPHERE RADII MEASURED USING LY α AND H I OBSERVATIONS

The most natural place to search for the redshifted 21cm signature of quasar H II regions is around the highest redshift quasars discovered in wide field surveys such as the *Sloan Digital Sky Survey* (SDSS⁶). Such quasars have H II regions that are also probed via their Ly α absorption spectra. In this section we discuss the complimentary nature of the two observations with respect to the determination of the quasar lifetime, $t_{\text{age,e}}$, and the neutral fraction of the IGM, x_{HI} .

Strömgren spheres expand faster into a partially ionized IGM. If the IGM has a neutral fraction x_{HI} , then the observation of R_{Ly} through Ly α absorption measures the combination $(t_{\text{age,e}}/x_{\text{HI}})^{1/3}$ (where here we have neglected recombinations and assumed $R_0 = 0$ for simplicity). Detection of the redshifted 21cm ring reflects the state of the H II region at $t_{\text{age,e}}$. The differential antenna temperature δT_{b} is proportional to x_{HI} due to the small optical depth at 21 cm,

$$\delta T_{\text{b}} \propto (1 - e^{-\tau_{\text{HI}}}) \approx \tau_{\text{HI}} \propto x_{\text{HI}}. \quad (20)$$

Measurement of the contrast in the emission and absorption rings, or of the brightness temperature of the emission ring, will facilitate a measurement of x_{HI} independent from $t_{\text{age,e}}$. Redshifted 21cm observations may therefore provide an opportunity to break the degeneracy between $t_{\text{age,e}}$ and x_{HI} . Unfortunately, the heating rate and temperature of the IGM are uncertain, and unless $T_{\text{k}} \gg T_{\text{CMB}}$, the value of δT_{b} will be sensitive to the unknown value of T_{k} . Below we discuss an alternative geometric method for finding x_{HI} that is not sensitive to the precise value of δT_{b} .

The relativistic expansion and finite light travel time imply that the 21cm and Ly α measurements sample two different epochs in the evolution of the H II region. The situation is illustrated schematically in figure 1. Suppose that the quasar turns on at t_0 , emitting photons isotropically into an existing H II region of radius R_0 . Ly α photons

emitted at t_0 will reach the edge of the H II region at t_1 . At that time, 21cm photons with $\delta T_{\text{b}} > 0$ are emitted by the heated gas at $R > R_0$ and travel towards the observer. For simplicity consider 21cm photons that are emitted from the heated IGM just beyond the ionizing front and perpendicular to the line-of-sight (i.e. at the quasar redshift). The sphere continues to expand at nearly the speed of light between t_1 and t_3 . At t_3 , the Ly α photons emitted at t_1 reach the edge of the H II region. The absorption of these photons encodes a measurement of R_3 . The continuum and 21cm photons propagate to the observer, who measures a radius R_3 along the line-of-sight in Ly α absorption, and a different radius R_0 in redshifted 21cm photons.

In this paper we define R_{Ly} to be the radius measured through Ly α absorption along the line-of-sight. This is compared with R_{HI} , defined to be the radius of the ring measured perpendicular to the line of sight through redshifted 21cm emission. The radii R_{Ly} and R_{HI} are not equal for a spherical region due to finite light travel time effects mentioned in the previous paragraph. We note that this effect is separate from the super-luminal transverse expansion of the ring of 21cm emission from the relativistically expanding portions of the H II region near the line-of-sight. These super-luminally expanding rings would be seen $\sim 3000\text{km s}^{-1}$ blueward of the quasar redshift (for $R_{\text{p}} \sim 4\text{Mpc}$).

The exact redshift of the quasar may be uncertain by up to $\sim 1000\text{km s}^{-1}$ (Richards et al. 2002). However this uncertainty corresponds to only 30% of the diameter of the H II region ($\sim 3000\text{km s}^{-1}$). A point on the edge of the H II region that is blueshifted by $\sim 1000\text{km s}^{-1}$ relative to the quasar lies in a direction away from the quasar that makes an angle of $\beta \sim \cos^{-1}(1000\text{km s}^{-1}/3000\text{km s}^{-1}) \sim 70^\circ$ with the line-of-sight. As a result, the misidentification of the quasar redshift will lead to an error of $\sim R_{\text{p}}(1 - \sin \beta) \sim 0.05R_{\text{p}}$ in the transverse diameter of the ring at the quasar redshift. Moreover, since $\beta \gtrsim 70^\circ$, the ring of 21cm emission at the observed quasar redshift

⁶ See <http://www.sdss.org/>

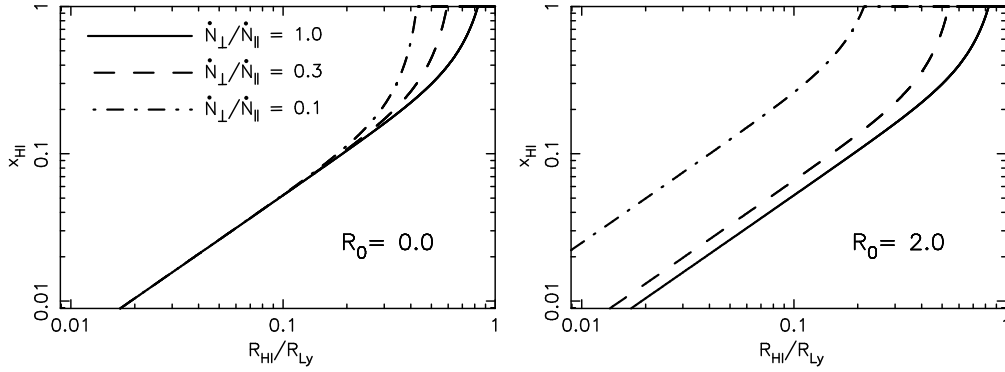


FIG. 2.— The neutral fraction as a function of the ratio $R_{\text{HI}}/R_{\text{Ly}}$ calculated from equation (24). The calculations are for the case where $R_{\text{Ly}} = 4.5\text{Mpc}$, $z = 6.5$ and $\dot{N}_{\parallel} = 10^{57}\text{s}^{-1}$. We show curves for $\dot{N}_{\perp}/\dot{N}_{\parallel} = 1.0, 0.3$ and 0.1 , and for $R_0 = 0$ (left hand panel) and $R_0 = 2$ (right hand panel).

will not be subjected to superluminal expansion, even if the quasar redshift is misidentified by $\sim 1000\text{km s}^{-1}$.

More quantitatively, the relativistic expansion and finite light travel time lead to several interesting possibilities:

- The coupling of the spin temperature of neutral hydrogen to the temperature of the warm IGM surrounding the H II region results in redshifted 21cm radiation in excess of the CMB. R_{HI} is measured transverse to the line-of-sight and so corresponds to the radius at the time the observed UV photons were emitted. We can directly infer the ionizing photon rate (\dot{N}_{\parallel}) which drives the evolution of the H II region along the line of sight. However, since the quasar emission may not be isotropic, we allow the evolution of the H II region transverse to the line of sight to be driven by a different ionizing photon rate \dot{N}_{\perp} . Thus, the ratio $\dot{N}_{\perp}/\dot{N}_{\parallel}$ is a measure of the anisotropy in quasar emission. Since high-redshift quasars are brightness selected, we assume that $\dot{N}_{\perp}/\dot{N}_{\parallel} \leq 1$. Using equation (3), we find the age of the quasar when light crossing the edge of the H II region was emitted ($t_{\text{age},e}$) and substitute it into equation (1) for the radius of the H II region *at that time*. This yields the following relationship between R_{Ly} and R_{HI}

$$R_{\text{Ly}}^3 = R_0^3 \left(\frac{\dot{N}_{\parallel}}{\dot{N}_{\perp}} - 1 \right) + R_{\text{HI}}^3 \left(\frac{\dot{N}_{\parallel}}{\dot{N}_{\perp}} \right) + \frac{R_{\text{HI}}}{c} \frac{3}{4\pi} \frac{\dot{N}_{\parallel}}{x_{\text{HI}} n_{\text{H}}^0 (1+z)^3}, \quad (21)$$

or

$$\left(\frac{R_{\text{HI}}}{R_{\text{Ly}}} \right)^3 = \left(\frac{\dot{N}_{\perp}}{\dot{N}_{\parallel}} \right) - \left(\frac{R_0}{R_{\text{Ly}}} \right)^3 \left(1 - \frac{\dot{N}_{\perp}}{\dot{N}_{\parallel}} \right) - \left[\left(\frac{R_{\text{HI}}}{R_{\text{Ly}}} \right) \left(\frac{R_{\text{Ly}}}{3.25\text{Mpc}} \right)^{-2} \times x_{\text{HI}}^{-1} \left(\frac{\dot{N}_{\perp}}{10^{57}\text{s}^{-1}} \right) \left(\frac{1+z}{7.5} \right)^{-3} \right] \quad (22)$$

Note that equations (21) and (22) are independent of R_0 when the quasar emission is isotropic, and that the dependence of $R_{\text{HI}}/R_{\text{Ly}}$ on $\dot{N}_{\perp}/\dot{N}_{\parallel}$

is rather mild. If the quasar emission is isotropic, the transverse radius R_{HI} is always smaller than the line-of-sight radius R_{Ly} , particularly during the relativistic expansion phase. When the expansion becomes sub-relativistic, R_{HI} approaches R_{Ly} .

- The radii measured through Ly α absorption and 21cm emission correspond to different epochs separated by R_{Ly}/c . For a spherical H II region we obtain the average expansion velocity of the ionizing front between the times corresponding to R_{HI} and R_{Ly}

$$\left\langle \frac{dR_p}{dt} \right\rangle = c \left(1 - \frac{R_{\text{HI}}}{R_{\text{Ly}}} \right). \quad (23)$$

Note that this velocity is the physical velocity of the ionizing front. The apparent transverse velocity of portions of the ring might be superluminal.

- Given a fixed luminosity, the expansion speed at a radius R_{Ly} is proportional to $x_{\text{HI}}^{-1/3}$, and so the neutral fraction can be inferred from the two radii. Equation (22) yields

$$x_{\text{HI}} = \left(\frac{R_{\text{Ly}}}{c} \frac{\dot{N}_{\parallel}}{n_{\text{H}}^0 (1+z)^3} \right) \times \left[\frac{4\pi}{3} \left(R_{\text{Ly}}^3 - R_{\text{HI}}^3 \left(\frac{\dot{N}_{\parallel}}{\dot{N}_{\perp}} \right) - R_0^3 \left(\frac{\dot{N}_{\parallel}}{\dot{N}_{\perp}} - 1 \right) \right) \right]^{-1} = \left[\frac{(R_{\text{HI}}/R_{\text{Ly}})}{1 - \left(\frac{R_{\text{HI}}}{R_{\text{Ly}}} \right)^3 \left(\frac{\dot{N}_{\parallel}}{\dot{N}_{\perp}} \right) - \left(\frac{R_0}{R_{\text{Ly}}} \right)^3 \left(\frac{\dot{N}_{\parallel}}{\dot{N}_{\perp}} - 1 \right)} \right]^{-1} \times \left(\frac{R_{\text{Ly}}}{3.25\text{Mpc}} \right)^{-2} \left(\frac{\dot{N}_{\parallel}}{10^{57}\text{s}^{-1}} \right) \left(\frac{1+z}{7.5} \right)^{-3} \quad (24)$$

Some examples of the dependence of x_{HI} on the ratio ($R_{\text{HI}}/R_{\text{Ly}}$) given $R_{\text{Ly}} = 4.5\text{Mpc}$ and $\dot{N}_{\parallel} = 10^{57}\text{s}^{-1}$, are shown in figure 2. In the case of isotropic quasar emission ($\dot{N}_{\perp}/\dot{N}_{\parallel} = 1$), a small ratio of ($R_{\text{HI}}/R_{\text{Ly}}$) implies relativistic expansion, and hence a small neutral fraction unless $R_{\text{Ly}} \ll 3.25\text{Mpc}$. Values of $\dot{N}_{\perp}/\dot{N}_{\parallel}$ which are less than

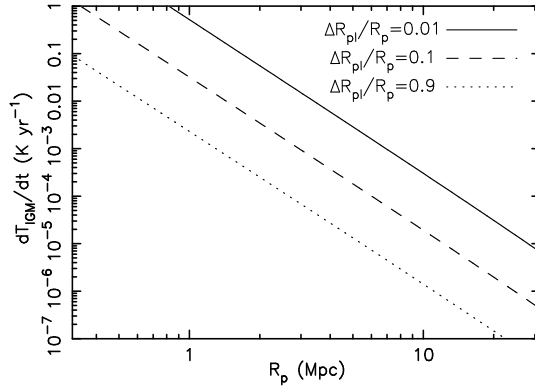


FIG. 3.— Plots of the heating rate of the IGM dT_{IGM}/dt (in K yr^{-1}) due to the X-ray emission by the quasar, as a function of the Strömgen radius. The three curves correspond to radii at which the photons have traversed H I path lengths of $\Delta R_{\text{pl}} = 0.01R_p$, $0.1R_p$ and $0.9R_p$, where R_p is the physical radius of the H II region. The assumed spectrum is given in equation (25), and the neutral fraction x_{HI} was set to unity.

unity lead to larger inferred values of x_{HI} . Similarly, a non-zero value for R_0 leads to larger values of x_{HI} . The assumptions of isotropy and $R_0 = 0$ lead to determination of a lower limit for x_{HI} . The observation of a redshifted 21cm ring with a radius greater than 2.5Mpc (0.5Mpc) around the known $z \gtrsim 6.3$ quasars (with $R_{\text{Ly}} \sim 4.5\text{Mpc}$) would provide a limit on the neutral fraction of $x_{\text{HI}} > 0.3$ ($x_{\text{HI}} > 0.05$).

4. SOME EXAMPLES

In this section we present examples of the redshifted 21cm signatures of $z > 6$ quasars that will be observed by instruments like *LOFAR*. The UV continuum blueward of $\text{Ly}\alpha$ is assumed to be that of the median spectrum in the sample of HST quasars studied by Telfer, Zheng, Kriss & Davidsen (2002). They found a power-law $\epsilon_c(\nu) \propto \nu^{-\alpha_{\text{EUV}}}$ with $\alpha_{\text{EUV}} = 1.57$. This slope may be extended into the X-ray regime based on the results of Yuan, Brinkmann, Siebert & Voges (1998). We include the $\text{Ly}\alpha$ emission line centered at $\lambda_\alpha = 912\text{\AA}$, with an equivalent width of $W_\lambda = 90\text{\AA}$ (Vanden Berk et al. 2001; Telfer, Zheng, Kriss & Davidsen 2002), and a line width of $\sigma_\lambda = 19\text{\AA}$ (Vanden Berk et al. 2001), providing a UV–X-ray spectrum

$$\epsilon(\nu) = 1.3 \times 10^{31} \text{erg s}^{-1} \text{Hz}^{-1} \left(\frac{\nu}{\nu_{\text{ion}}} \right)^{-\alpha_{\text{EUV}}} \times \left[1 + \frac{1}{\sqrt{2\pi}\sigma_\lambda} \exp\left(-\frac{(c/\nu - \lambda_\alpha)^2}{\sigma_\lambda^2} \right) \right]. \quad (25)$$

The normalization of this spectrum is appropriate for a $2 \times 10^9 M_\odot$ supermassive black hole accreting at its Eddington rate (Elvis et al. 1994), and it yields an ionizing photon rate of $\dot{N}_\parallel = 1.3 \times 10^{57} \text{s}^{-1}$, representative of the $z \gtrsim 6.3$ SDSS quasars (White et al. 2003). In this section, we show examples of the 21cm emission signal that may be observed around the known very high redshift quasars, with the spectrum described by equation (25).

The level of redshifted 21cm emission is enhanced through heating of the IGM by the quasar X-ray emission. The corresponding heating rates dT_{IGM}/dt of the above quasar spectrum are plotted as a function of radius in figure 3. The three curves correspond to radii where photons traversed path lengths through neutral gas

of $\Delta R_{\text{pl}} = 0.01R_p$, $0.1R_p$ and $0.9R_p$. The neutral fraction was set to unity in these examples. Note that lower neutral fractions lead to higher values of f_x and hence larger heating rates.

If the Strömgen spheres expand into a pre-heated IGM containing a UV background that coupled the spin temperature of the IGM to its kinetic temperature, the H II regions should appear as holes in the sky of redshifted 21cm emission. As an example we first consider an IGM that is pre-heated to $\sim 100\text{K}$ at $z = 6.3$ ($T_{\text{IGM}} \sim 5T_{\text{CMB}}$). We follow the evolution of the Strömgen sphere, and at each time compute the heating rate of the IGM beyond the edge of the H II region using equation (15). The evolution of the kinetic temperature of the IGM is followed on a grid using equation (17). The spin temperature is then set to T_{IGM} as appropriate in the presence of a strong $\text{Ly}\alpha$ background. Figure 4 shows four examples of the 21 cm emission signature of a Strömgen sphere expanding into a warm IGM as a function of radius (top axes) and apparent angle (bottom axes) for different combinations of $\dot{N}_\perp/\dot{N}_\parallel = 1.0, 0.1$ and $x_{\text{HI}} = 1.0, 0.1$. An initial value of $R_0 = 0$ was assumed. The y-axes are labeled by the differential antenna temperature δT_b (right axes), and the flux δI (left axes) assuming the design goal sensitivity of *LOFAR*

$$\delta I = (1.2 \mu\text{Jy arcmin}^{-2}) \left(\frac{\delta T_b}{10\text{mK}} \right) \left(\frac{1+z}{7.5} \right)^{-2}, \quad (26)$$

and a top-hat beam with a diameter of $2'$. In each case, four profiles are shown for observing times corresponding to quasar ages of $t_{\text{age,e}} = 0.5, 1, 2, 4 \times 10^7 \text{yr}$ at the time when the *optical photons* observed along the line-of-sight were emitted. The lower row includes cases with $x_{\text{HI}} = 0.1$. The smaller neutral fraction results in larger radii, faster relativistic expansion, and therefore thinner emission shells. The 21cm emission signal is weaker in this case because $\delta T_b \propto x_{\text{HI}}$. There is excess emission above the level of the general IGM in a ring covering the region where gas has been heated by the quasar. However the brightness temperature is only slightly higher than the rest of the IGM. This is due to the temperature dependence of ΔT_b which asymptotes to a constant value of $\sim 23x_{\text{HI}}\text{mK}$ for high temperatures. The panels on the right show examples with $\dot{N}_\perp/\dot{N}_\parallel = 0.1$. The lower transverse flux results

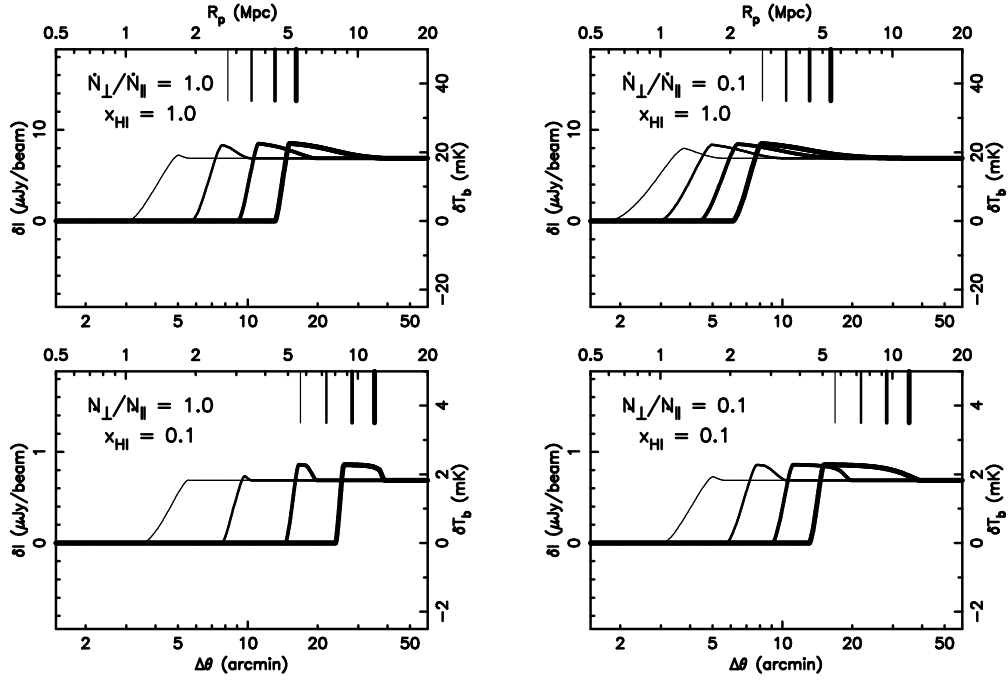


FIG. 4.— Four examples of the evolution of a Strömgen sphere expanding into a warm ($T_{\text{IGM}} = 5T_{\text{CMB}}$) IGM as seen in redshifted 21cm emission and Ly α absorption, assuming different combinations of $\dot{N}_{\perp}/\dot{N}_{\parallel} = 1.0, 0.1$ and $x_{\text{HI}} = 1.0, 0.1$. In all cases we assume $R_0 = 0$. The 21cm emission signal is plotted as a function of radius (upper horizontal axes) and apparent angle in arc-minutes (lower axes). The y-axes are labeled by the differential antenna temperature δT_b (right axes) and the flux δI (left axes) given a circular top-hat beam with a diameter of $2'$. In each case, four profiles are shown for observing times corresponding to quasar ages of $t_{\text{age},e} = 0.5, 1, 2, 4 \times 10^7$ yr when the *optical photons* were emitted. Values of R_{Ly} at $t_{\text{age},e} = 0.5, 1, 2, 4 \times 10^7$ yr are shown with tick marks.

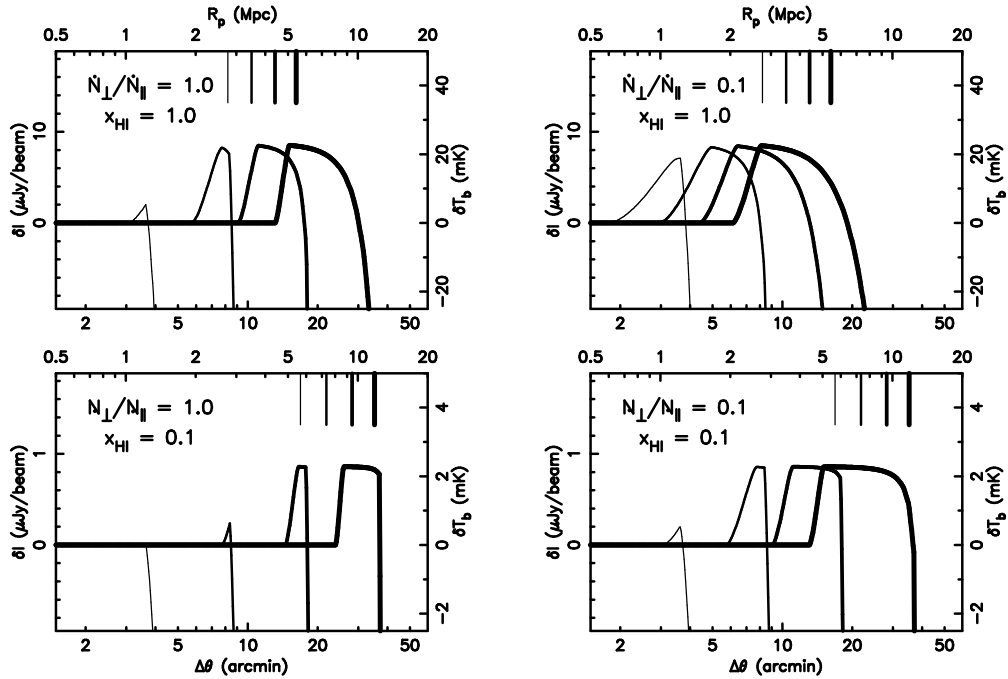


FIG. 5.— Same as in figure 4, but with a cold IGM having $T_{\text{IGM}} = 0.026(1+z)^2 \ll T_{\text{CMB}}$.

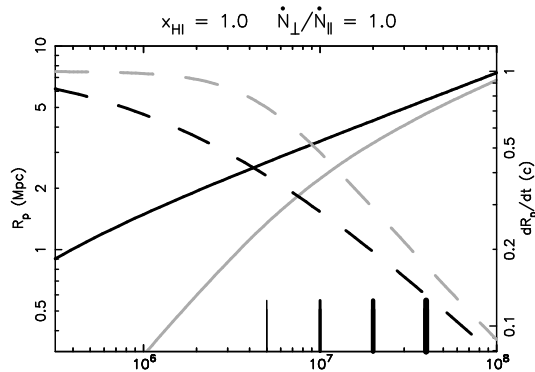


FIG. 6.— Plots of the radius measured through Ly α absorption along the line-of-sight $R_{\text{Ly}}(t_{\text{age}})$ (solid dark lines) as well as the radius of the interior boundary of the 21cm emission ring at the quasar redshift (solid light lines). The dashed lines show the speed at which the edge of the H II region seen in 21cm (light lines) and Ly α absorption (dark lines) is moving when observed at a time corresponding to $t_{\text{age},e}$. The curves correspond to the example shown in the top left panel of figures 4 with $\dot{N}_{\perp}/\dot{N}_{\parallel} = 1$ and $x_{\text{HI}} = 1$.

in an expansion that becomes sub-relativistic at earlier times. As a result, the emission shell has a smaller radius and a larger thickness.

As our second example we consider an IGM that is cold in neutral regions [$T \sim 0.026(1+z)^2$, corresponding to adiabatic cooling following the thermal decoupling of the baryons from the CMB]. The resulting 21 cm signal is shown in figure 5. The heated portions of the IGM beyond the edge of the H II region show emission, while the cold IGM produces absorption of the CMB at larger radii. The brightness temperature of the emission ring obtains values of $T_b \sim 20x_{\text{HI}}\text{mK}$, smaller in amplitude than the absorption signal of $T_b \sim -295x_{\text{HI}}\text{mK}$. A cold IGM therefore offers the best contrast for observation of the transverse extent of the H II region. As in the previous example, the emission rings get thicker at late times because the expansion speed becomes less relativistic. Since the transverse expansion becomes sub-relativistic sooner than the line-of-sight expansion, the rings become thick at earlier times for a lower value of $\dot{N}_{\perp}/\dot{N}_{\parallel}$.

Figure 6 shows $R_{\text{Ly}}(t_{\text{age}})$ (solid dark lines) as well as the inner radius of the 21cm emission ring (solid light lines) for the example presented in the top left panels of figures 4 and 5 ($\dot{N}_{\perp}/\dot{N}_{\parallel} = 1$, $x_{\text{HI}} = 1$). The four epochs corresponding to the differential antenna temperature profiles plotted in figures 4 and 5 are indicated by the vertical tick marks. Similarly, values of R_{Ly} at $t_{\text{age},e} = 0.5, 1, 2, 4 \times 10^7\text{yr}$ are indicated by tick marks in the panels of figures 4 and 5. The value of R_{Ly} is always larger than the radius of 21cm emission. The dashed lines show the velocity at which the edge of the H II region is moving when observed at a time corresponding to $t_{\text{age},e}$. The 21cm ring (light dashed lines) is observed at an earlier phase of evolution and so is moving at a higher velocity. The edge of the H II region is moving at a speed $\gtrsim 0.2c$ when $R_p \lesssim 4.5\text{Mpc}$.

5. FOSSIL H II REGIONS IN THE HIGH REDSHIFT IGM

The presence of a Ly α background has very interesting implications for the observation of fossil H II regions. The recombination time within an ionized region of the IGM at mean density is $t_{\text{recom}} \sim (\alpha_{\text{B}}n_{\text{H}}^0(1+z)^3)^{-1} \sim 1.5 \times 10^9[(1+z)/7.5]^{-3}$ years, where $\alpha_{\text{B}} = 2.6 \times 10^{-13}\text{cm}^3\text{s}^{-1}$ is the case-B recombination coefficient at a temperature of 10^4K . Thus, the recombination time at the mean cosmic

density exceeds the Hubble time for $z \lesssim 7$. Once a quasar has turned off, it therefore leaves behind a fossil H II region that survives recombination. This H II region will therefore remain detectable in redshifted 21cm radiation in both scenarios discussed in this paper. Since the bright SDSS quasars are likely to be active for only $\sim 1\%$ of the time (Wyithe & Loeb 2003b), there should be of order 100 times as many 21cm emission rings around fossil H II regions as around active quasars. Furthermore, the hierarchical buildup of the supermassive black holes powering the quasars would result in an even larger number of small fossil H II regions.

How many H II regions should an instrument like *LO-FAR* detect? It is anticipated that near frequencies of $\nu_{\text{bp}} \sim 200\text{MHz}$, the virtual core of the planned instrument *LOFAR* will have a beam-size of $\Delta\theta_{\text{beam}} \sim 23^\circ$, a resolution of several tens of arc-minutes, and a system temperature of $T_{\text{sys}} \sim 300\text{K}$. The instrument will have an effective collecting area of $A \sim 10^5\text{m}^2$ at this frequency, leading to a resolution of $\Delta\theta_{\text{fa}} \sim 1.22\lambda\sqrt{\pi/A} \sim 22'$ for the telescope in a filled aperture mode. Higher resolutions are obtained by spreading the array out over longer baselines, at the cost of decreased sensitivity. From the radiometer equation (e.g. Burke & Graham-Smith 1997) we can find the root-mean-square noise in the brightness temperature as a function of resolution on angular scales $\Delta\theta < \Delta\theta_{\text{fa}}$ of

$$\begin{aligned} \Delta T_b(\Delta\theta) &= (0.24\text{mK}) \left(\frac{\Delta\theta}{\Delta\theta_{\text{res}}} \right)^2 \left(\frac{T_{\text{sys}}}{300\text{K}} \right) \\ &\times \left(\frac{\Delta\nu_{\text{bp}}}{4\text{MHz}} \right)^{-1} \left(\frac{\tau}{100\text{hr}} \right)^{-1/2} \end{aligned} \quad (27)$$

Here $\Delta\nu_{\text{bp}}$ is the detector band-pass, and τ is the integration time. The noise in the brightness temperature is constant on scales larger than $\Delta\theta_{\text{fa}}$. The root-mean-square noise for an observation with a resolution $\Delta\theta \sim 3'$ therefore becomes comparable to the expected emission signal ($\delta T_b \sim 10\text{mK}$) for a modest integration time of $\tau \sim 100\text{hr}$.

The co-moving optical luminosity function of bright quasars at $z \sim 6$ in units of $L_{\odot}^{-1}\text{Gpc}^{-3}$ (Fan et al. 2003) is

$$\Phi(L) \approx 10^{-13}L_{\odot}^{-1}\text{Gpc}^{-3} \left(\frac{L}{10^{13.1}L_{\odot}} \right)^{\beta}, \quad (29)$$

where $\beta \sim -3$ is the logarithmic slope at the bright end. Given a band-pass $\Delta\nu_{\text{bp}} \sim 4\text{MHz}$ and a central frequency $\nu_{\text{bp}} \sim 200\text{MHz}$, the number of active quasars per logarithm of luminosity per field of view is

$$N \sim L\Phi(L) \frac{d^2V}{dzd\Omega} \pi \left(\frac{\Delta\theta_{\text{beam}}}{2} \right)^2 (1+z) \frac{\Delta\nu_{\text{bp}}}{\nu_{\text{bp}}}, \quad (30)$$

where $d^2V/dz d\Omega$ is the co-moving volume per unit redshift per unit solid angle. Equation (30) yields a value of $N \sim 2$ bright $z \sim 6$ quasars per *LOFAR* field.

The number of redshifted 21cm rings or holes in the emission signature of the IGM per field as determined by equation (30) applies to active quasars. However as noted above, the 21cm emission may persist after the quasar has turned off. This is because in the absence of other heating sources, gas heated to temperatures far in excess of the CMB will cool adiabatically. The $(1+z)^2$ dependence of the temperature in this regime should ensure that the gas remains at a temperature in excess of the CMB by the time it is re-heated during the next episode of quasar activity. We might expect to find significant numbers of fossil H II regions, provided that there is continued coupling of T_s and T_{IGM} due to a UV background. The number of detectable fossil H II regions would then equal the number in equation (30) multiplied by the inverse of the quasar duty cycle $\sim 1\%$ (Wyithe & Loeb 2003b), or about 200 per field.

LOFAR should also be sensitive to H II regions around less luminous quasars. The brightness temperature of the emission ring, or of the IGM outside the H II region has a mild dependence on the quasar luminosity, and its diameter scales only with the one third power of the luminosity. H II regions around less luminous quasars should be more numerous by a factor proportional to $L^{\beta+1}$. For example, detection of redshifted 21cm emission around quasars with luminosities a factor of 10 smaller than those of the bright SDSS quasars require a resolution that is better by a factor of $10^{1/3}$, corresponding to an integration time that is longer by a factor of $10^{2/3} \sim 4.6$. However, the number of active high redshift quasars per field powering such emission rings is likely to be of order $10^2 N \sim 200$, while the number of fossils regions could be $\sim 2 \times 10^4$.

Finally, we briefly discuss the example of a redshifted 21cm signature around a high redshift quasar presented in 5b of Tozzi et al. (2000). Their example shows a ring of redshifted 21cm emission inside a ring of redshifted 21cm absorption. This morphology is unlikely to be observed because the observation of an absorption ring requires the absence of a UV background, and the provision of coupling of the spin and kinetic temperatures through Ly α photons from the quasar itself. As we have shown, Ly α photons from the quasar are unable to couple the spin and kinetic temperatures. An emission ring enclosed within an IGM that absorbs everywhere, as shown in figure 5 is the correct signature of a Strömgen sphere expanding into a cold IGM (provided that there is a UV background).

6. STRÖMGREN SPHERES AND THE GLOBAL SIGNATURE OF REIONIZATION

A very exciting possibility for instruments like *LOFAR* is to search for the emission (or absorption) of redshifted 21cm radiation from the neutral IGM (averaged over large

scales) before reionization. By finding the frequency at which this emission (absorption) cuts off, one might determine the redshift of reionization (e.g. Shaver et al. 1999). If reionization took place over an extended period of time as suggested by recent work (Barkana & Loeb 2003b), then this global reionization signature will be difficult to detect for two primary reasons: (i) because it will be superimposed on a smooth but varying foreground spectrum, and (ii) calibration needs to be performed over a frequency range that is broader than the detector band-pass.

Arc-minute resolution observations of quasar Strömgen spheres would provide an alternative method to search for a step in the brightness temperature of the IGM due to reionization. This is because the inner part of the H II region provides a calibration of the brightness temperature of the radio foreground that is unavailable along other lines of sight. Note that 21cm emission from the quasar itself does not affect this calibration, since it effectively just adds to the foreground. Observations along the line-of-sight to the quasar would include emission within the spectral ranges corresponding to both the ionized region and the neutral gas within the same band-pass. Redshifted 21cm observations of quasars at a series of redshifts would therefore allow determination of the brightness temperature of the IGM at different cosmic times, and a detection of the onset of reionization. Redshifted 21cm observation of highest-redshift SDSS quasars will immediately determine whether the IGM was significantly neutral at $z > 6.3$.

7. DISCUSSION

Observations of the reionization epoch in redshifted 21cm radiation with proposed instruments like *LOFAR* will offer a unique opportunity to study the state of the IGM at the end of the dark ages. The warm neutral hydrogen outside the H II regions surrounding bright high redshift quasars is expected to emit at 21cm. The brightness temperature contrast of this emission will probe the neutral fraction (with a lower contrast implying a lower neutral fraction), although the inference will be subject to uncertainties in the temperature of the warm IGM. Alternatively, the relativistic expansion of the H II regions provides a geometric method to determine the neutral fraction as well as the quasar lifetime.

We have combined the observed Ly α absorption signal with expectations for redshifted 21cm signatures of the H II regions around the highest redshift SDSS quasars. Because the H II regions around the known $z \gtrsim 6.3$ quasars are at a stage of relativistic expansion, the line-of-sight and transverse radii (measured through Ly α absorption and redshifted 21cm emission, respectively), correspond to two different epochs in the evolution of the H II regions. We have found that measurements of these two radii can be used to determine the neutral fraction of the IGM with only a mild dependence on the anisotropy of the quasar emission (see Fig. 2). Assuming isotropic quasar emission and the absence of a fossil H II region prior to the quasar activity, the observation of a redshifted 21cm emission ring with a radius greater than 2.5Mpc (0.5Mpc) around the known $z \gtrsim 6.3$ quasars, would provide a lower limit on the neutral fraction of $x_{\text{HI}} > 0.3$ ($x_{\text{HI}} > 0.05$). Emission concentrated close to the line-of-sight and the existence of fossil H II regions around the quasar host galaxy would

imply even larger neutral fractions.

At low redshifts, quasar lifetimes are bracketed by a variety of techniques to the range $\sim 10^6$ – 10^8 yr (e.g. Yu & Tremaine 2002; Martini & Weinberg 2001; Haiman & Hui 2001; Jakobsen, Jansen, Wagner & Reimers 2003), with preferred values near 10^7 years (e.g. Martini 2003). The lifetime required for the H II region to expand to its observed size is proportional to $x_{\text{HI}}^{-1/3}$. The geometric determination of the neutral fraction can therefore be directly used to determine also the quasar lifetime measured from the combination of R_p and x_{HI} . Thus, Ly α and redshifted 21cm measurements of the expanding H II regions around the highest redshift quasars will allow a direct determination of quasar ages on a case by case basis and constrain quasar formation models (e.g. Haiman & Loeb 2001).

Based on current number counts of bright high redshift quasars and the preliminary design of *LOFAR*, we forecast that each *LOFAR* field (of radius $\sim 11^\circ$) will contain ~ 2 active quasars as bright as the observed SDSS quasars within one band-pass of frequency (~ 4 MHz). An integration time of ~ 100 hours should be sufficient to detect the rings of redshifted 21cm emission from the warm IGM outside the quasar H II regions if $x_{\text{HI}} = 1$. In the presence of a strong cosmic Ly α background, these rings should remain visible after the quasar has turned off. This would result in the detection of a large number of fossil H II regions that exceeds the number of active quasars by the inverse of the quasar duty cycle (~ 100).

Arc-minute observations of quasar Strömgen spheres will provide an alternative method for measuring the spectral step that makes the so-called global signature of reionization (Shaver et al. 1999). The brightness temperature measured in the spectral range corresponding to the ionized gas within the H II region provides a calibration of the foreground emission at the same redshift. This calibration will help overcome the difficulties associated with measuring the global signature of an extended reionization epoch (as suggested by the large electron scattering optical depth measured by *WMAP*; Kogut et al. 2003) on top of a frequency dependent foreground. Detection of the signal for a statistical sample of quasars would help calibrate the expected scatter in the reionization redshift of different regions in the universe (Barkana & Loeb 2003b).

Finally, we emphasize that the redshifted 21cm observation of existing SDSS quasars will determine whether the IGM was significantly neutral at $z > 6.3$ as suggested by their observed Ly α spectra (Wyithe & Loeb 2004). When combined with the high value of the optical depth for electron scattering measured by *WMAP* (Kogut et al. 2003), a significant neutral fraction at $z \sim 6.3$ would imply a complex reionization history and possibly an early reionization phase driven by Population-III stars.

This work was supported in part by NASA grant NAG 5-13292, and by NSF grants AST-0071019, AST-0204514 (for A.L.).

REFERENCES

- Barkana, R., & Loeb, A., 2003a, ApJ, in press; astro-ph/0305470
 Barkana, R., & Loeb, A., 2003b, ApJ, submitted; astro-ph/0310338
 Burke, B. F. & Graham-Smith, F. 1997, Infrared Astronomy, Cen, R. 2003, ApJ, 591, 12
 Cen, R. & Haiman, Z. 2000, ApJ, 542, L75
 Chen, X., Miralda-Escudé, J., 2003, astro-ph/0303395
 Ciardi, B. & Madau, P. 2003, ApJ, 596, 1
 Di Matteo, T., Perna, R., Abel, T., & Rees, M. J. 2002, ApJ, 564, 576
 Fan, X. et al. 2003, AJ, 125, 1649
 Field, G.B., 1958, Proc. IRE, 46, 240
 Furlanetto, S., & Loeb, A. 2003, ApJ, submitted
 Furlanetto, S., Sokasian, A., & Hernquist, L. 2003, MNRAS, submitted; preprint astro-ph/0305065
 Gnedin, N. Y. & Ostriker, J. P. 1997, ApJ, 486, 581
 Gnedin, N., Shaver, P.A., 2003, astro-ph/0312005
 Haiman, Z. & Hui, L. 2001, ApJ, 547, 27
 Haiman, Z. & Loeb, A. 2001, ApJ, 552, 459
 Iliev, I. T., Shapiro, P. R., Ferrara, A., & Martel, H. 2002, ApJ, 572, L123
 Iliev, I. T., Scannapieco, E., Martel, H., & Shapiro, P. R. 2003, MNRAS, 341, 81
 Jakobsen, P., Jansen, R., A., Wagner, S., Reimers, D., 2003, Astron. Astrophys, 397, 891
 Kogut, A. et al. 2003, ApJS, 148, 161
 Shaver, P. A., Windhorst, R. A., Madau, P., & de Bruyn, A. G. 1999, A&A, 345, 380
 Loeb, A. & Rybicki, G. B. 1999, ApJ, 524, 527
 Loeb, A., & Zaldarriaga, M. 2003, Phys. Rev. Lett., submitted; preprint astro-ph/0312134
 Madau, P., Meiksin, A., & Rees, M. J. 1997, ApJ, 475, 429
 Madau, P. & Rees, M. J. 2000, ApJ, 542, L69
 Martini, P. & Weinberg, D. H. 2001, ApJ, 547, 12
 (18) Martini, P. 2003, preprint astro-ph/0304009
 Oh, S.P., Mack, K.J., 2003, astro-ph/0302099
 Richards, G.T., Vanden Berk, D.E., Reichard, T.A., Hall, P.B., Schneider, D.P., SubbaRao, M., Thakar, A.R., York, D.G., Astron. J. Supp., 124, 1
 Rybicki, G. B. & Lightman, A. P. 1979, (New York, Wiley-Interscience), p. 288
 Scott, D. & Rees, M. J. 1990, MNRAS, 247, 510
 Shaver, P. A., Windhorst, R. A., Madau, P., & de Bruyn, A. G. 1999, A&A, 345, 380
 Shull, J. M. & van Steenberg, M. E. 1985, ApJ, 298, 268
 Spergel, D. N. et al. 2003, ApJS, 148, 175
 Telfer, R. C., Zheng, W., Kriss, G. A., & Davidsen, A. F. 2002, ApJ, 565, 773
 Tozzi, P., Madau, P., Meiksin, A., & Rees, M. J. 2000, ApJ, 528, 597
 Vanden Berk, D. E. et al. 2001, AJ, 122, 549
 White, R. L., Becker, R. H., Fan, X., & Strauss, M. A. 2003, astro-ph/0303476
 Wouthuysen, S.A., 1952, Astron. J., 57, 31
 Wyithe, J. S. B. & Loeb, A. 2003a, ApJ, 586, 693
 Wyithe, J. S. B. & Loeb, A. 2003b, ApJ, 595, 614
 Wyithe, J. S. B., & Loeb, A. 2004, Nature, accepted
 Yu, Q. & Tremaine, S. 2002, MNRAS, 335, 965
 Yuan, W., Brinkmann, W., Siebert, J., & Voges, W. 1998, A&A, 330, 108
 Zaldarriaga, M., Furlanetto, S., & Hernquist, L. 2003, ApJ, submitted; preprint astro-ph/0311514